3-2000

Parity Violation in Neutron Resonances in 115In

Sharon L. Stephenson
Gettysburg College

J D. Bowman
Los Alamos National Laboratory

J Corvi
Institute for Reference Materials and Measurements

See next page for additional authors

Stephenson, S., Bowman, J. D., Corvi, J., Crawford, B. E., Delheij, P. P. J., Frankle, C. M., IInuma, M., Knudsen, J. N., Lowie, L. Y., Masaike, A., Masuda, Y., Matsuda, Y., Mitchell, G. E., Penttila, S. I., Postma, H., Roberson, N. R., Seestrom, S. J., Sharapov, E. I., Shimizu, H. M., Yen, Y-F., Yuan, V. W., & Zanini, L. (2000). Parity Violation in Neutron Resonances in 115In. Physical Review C, 61(045501). http://dx.doi.org/10.1103/PhysRevC.61.045501

Parity Violation in Neutron Resonances in 115In

Abstract

Parity nonconservation (PNC) was studied in p-wave resonances in indium by measuring the helicity dependence of the neutron total cross section in the neutron energy range 6.0–316 eV with the time-of-flight method at LANSCE. A total of 36 p-wave neutron resonances were studied in ^{115}In, and statistically significant asymmetries were observed for nine cases. An analysis treating the PNC matrix elements as random variables yields a weak matrix element of $M=(0.67_{-0.12}^{+0.16})$ meV and a weak spreading width of $\Gamma_w=(1.30_{-0.43}^{+0.76})\times10^{-7}$ eV.

Disciplines

Atomic, Molecular and Optical Physics | Physics

Authors

Sharon L. Stephenson, J D. Bowman, J Corvi, Bret E. Crawford, P P J. Delheij, C M. Frankle, M IInuma, J N. Knudsen, L Y. Lowie, A Masaike, Y Matsuda, G E. Mitchell, S I. Penttila, H Postma, N R. Roberson, S J. Seestrom, E I. Sharapov, H M. Shimizu, Y-F Yen, V W. Yuan, and L Zanini

Parity violation in neutron resonances in ^{115}In

S. L. Stephenson,[1,*] J. D. Bowman,[2] F. Corvi,[3] B. E. Crawford,[4,*] P. P. J. Delheij,[5] C. M. Frankle,[2] M. Iinuma,[6,†] J. N. Knudson,[2] L. Y. Lowie,[1,‡] A. Masaike,[6,§] Y. Masuda,[7] Y. Matsuda[6,‖] G. E. Mitchell,[1] S. I. Penttilä,[2] H. Postma,[8] N. R. Roberson,[4] S. J. Seestrom,[2] E. I. Sharapov,[9] H. M. Shimizu,[7,¶] Y.-F. Yen[2,**] V. W. Yuan,[2] and L. Zanini[3,††]

[1]*North Carolina State University, Raleigh, North Carolina 27695-8202*
and Triangle Universities Nuclear Laboratory, Durham, North Carolina 27708-0308
[2]*Los Alamos National Laboratory, Los Alamos, New Mexico 87545*
[3]*Institute for Reference Materials and Measurements, Geel, Belgium*
[4]*Duke University, Durham, North Carolina 27708*
and Triangle Universities Nuclear Laboratory, Durham, North Carolina 27708-0308
[5]*TRIUMF, Vancouver, British Columbia, Canada V6T 2A3*
[6]*Physics Department, Kyoto University, Kyoto 606-01, Japan*
[7]*National Laboratory for High Energy Physics, 1-1, Oho, Tsukuba 305, Japan*
[8]*Delft University of Technology, IRI/ISO, 2629 JB, Delft, the Netherlands*
[9]*Joint Institute for Nuclear Research, 141980 Dubna, Russia*

(Received 28 September 1999; published 6 March 2000)

Parity nonconservation (PNC) was studied in *p*-wave resonances in indium by measuring the helicity dependence of the neutron total cross section in the neutron energy range 6.0–316 eV with the time-of-flight method at LANSCE. A total of 36 *p*-wave neutron resonances were studied in ^{115}In, and statistically significant asymmetries were observed for nine cases. An analysis treating the PNC matrix elements as random variables yields a weak matrix element of $M=(0.67^{+0.16}_{-0.12})$ meV and a weak spreading width of $\Gamma_w=(1.30^{+0.76}_{-0.43})\times 10^{-7}$ eV.

PACS number(s): 24.80.+y, 25.40.Ny, 27.60.+j, 11.30.Er

I. INTRODUCTION

After the Dubna team discovery [1] of large parity violation for neutron resonances in heavy nuclei, the Time Reversal Invariance and Parity at Low Energies (TRIPLE) Collaboration initiated a program to study parity violation in compound nuclei, using the high neutron flux available at the Manuel Lujan Jr. Neutron Scattering Center at the Los Alamos Neutron Science Center (LANSCE). A statistical ansatz was adopted: the compound nucleus is considered a statistical system and the symmetry-breaking matrix elements as random variables. In this approach the result of a parity nonconservation (PNC) experiment is the root-mean-square symmetry-breaking matrix element which is obtained from a set of longitudinal asymmetries $\{p\}_E$ measured for many resonances. For a particular resonance at energy E, the asymmetry p is defined by the equation

$$\sigma^{\pm}(E)=\sigma_p(E)(1\pm p), \tag{1}$$

where $\sigma^{\pm}(E)$ is the neutron cross section for the + and − neutron helicity states, and $\sigma_p(E)$ is the *p*-wave resonance cross section for unpolarized neutrons. Results from the early measurements are discussed in the reviews by Bowman *et al.* [2], Frankle *et al.* [3], and Flambaum and Gribakin [4]. After the initial measurements we improved the experimental system, repeated and improved the early measurements, and carried out experiments with additional targets. The most recent review is by Mitchell *et al.* [5].

In practice the parity violation measurements are feasible only near a maximum of the *p*-wave neutron strength function. The initial TRIPLE measurements with ^{232}Th and ^{238}U were near the maximum of the $4p$ neutron strength function, and thus gave no information concerning any mass dependence in the effective nucleon-nucleus weak interaction. Therefore our attention turned to the mass $A=110$ region, where the $3p$ neutron strength function maximum is located. We performed measurements on a number of targets from this region, and results have been published for several nuclei: ^{93}Nb [6], ^{103}Rh [7], ^{107,109}Ag [8], ^{113}Cd [9], and ^{133}Cs [10]. This approach was successful; many PNC effects were observed for almost all odd mass targets that we studied near the $3p$ neutron strength function maximum. However, a complication arises in the analysis of these data. As discussed below, it is important to have spectroscopic information (including spins) for the *s*- and *p*-wave resonances. Absent such spectroscopic information one can proceed by averaging over the various possibilities, but this often intro-

*Present address: Gettysburg College, Gettysburg, PA 17325.
†Present address: Hiroshima University, Hiroshima-Ken 739-8526, Japan.
‡Present address: McKinsey and Company, Atlanta, GA 30303.
§Present address: Fukui University of Technology, 3-6-1 Gakuen, Fukui-shi, 910-8505, Japan.
‖Present address: Institute of Physical and Chemical Research (RIKEN), 2-1 Hirosawa, Wako, Saitama, 351-8526, Japan.
¶Present address: Institute of Physical and Chemical Research (RIKEN), 2-1 Hirosawa, Wako, Saitama, 351-0198, Japan.
**Present address: Wake Forest University School of Medicine, Winston-Salem, NC 27157.
††Present address: Los Alamos National Laboratory, Los Alamos, New Mexico 87545.

duces a large uncertainty into the value for the rms PNC matrix element. In the present paper we report the PNC study on ^{115}In. These measurements form part of the Ph.D. dissertation of Lowie [11]. In addition, we present the resonance spin assignments from measurements performed at the Institute for Reference Materials and Measurements (IRMM). These latter measurements form part of the Ph.D. dissertation of Zanini [12].

In Sec. II the experimental methods for these two measurements are described, while the data analysis is discussed in Sec. III. The experimental results are presented in Sec. IV. The analysis for the extraction of the PNC matrix elements and weak spreading widths is described and the results for indium are given in Sec. V. The final section presents a brief summary.

II. EXPERIMENTAL METHODS

A. Parity violation

Transmission measurements of PNC asymmetries p were performed at the Manuel Lujan Jr. Neutron Scattering Center (MLNSC) pulsed neutron source. This spallation source is described by Lisowski *et al.* [13]. The apparatus developed by TRIPLE to measure p is described in a number of papers: including the original experimental layout [14], neutron monitor [15], polarizer [16], spin flipper [17], and neutron detector [18]. The layout of the polarized neutron beam line for the present PNC experiments is given in Ref. [8]. The measurements were performed on flight path 2, which views a gadolinium-poisoned water moderator and has a cadmium/boron liner to reduce the number of low-energy neutrons emerging in the tail of the neutron pulse. After the moderator the neutrons are collimated to a 10-cm-diam beam inside a 5-m-thick biological shield. The neutrons then pass through a ^{3}He/^{4}He ion chamber system [15] that acts as a flux monitor. The neutron flux is measured by the monitor for each neutron burst, and these measurements are used to normalize the detector rates. Next, the neutrons traverse a polarized-proton spin filter [16] where neutrons with one of the two helicity states preferentially scatter out of the beam, leaving a beam of longitudinally polarized neutrons (with the value of polarization $f_n \simeq 70\%$). The fast neutron spin reversal (every 10 s) was accomplished by passing the neutron beam through a spin flipper consisting of a system of magnetic fields [17]. In addition to frequent spin reversal, the neutron spin was also flipped by reversing the polarization direction of the proton spin filter approximately every 2 days. The total effective production time for indium data was 8 days.

The PNC effects in indium were measured by transmitting the neutron beam through samples located at the downstream part of the spin flipper. We used two samples of natural indium with $n = 2.88 \times 10^{23}$ atoms/cm^2 and $n = 5.86 \times 10^{23}$ atoms/cm^2, respectively. The measurements were performed both at room temperature and at 77 K. The ^{10}B-loaded liquid scintillation detector [18] is located 56.7 m from the neutron source. The 55-cell segmented detector can handle instantaneous counting rates up to 9 MHz per cell with a dead time of about 20 ns. The detector has an efficiency of 95%, 85%, and 71% at neutron energies of 10 eV, 100 eV, and 1000 eV, respectively. The neutron mean capture time in the detector is (416 ± 5) ns. The data acquisition process is initiated with each proton burst. The detector signals are linearly summed and filtered. An analog-to-digital converter (ADC) transient recorder digitally samples the summed detector signal 8192 times in intervals determined by the filtering time. The 8192 words are added, as a ''pass,'' to a summation memory for 200 beam bursts before being stored. The data from 160 passes form a 30-min ''run'' for the data analysis. For indium 162 runs with a channel width of 100 ns were used in the final analysis. In addition, 34 runs were measured and analyzed with a channel width of 200 ns.

B. Spin determination

Measurements to determine resonance spins in ^{115}In were performed at the Geel Linac pulsed neutron source facility using the time-of-flight (TOF) technique [12]. The experimental setup was the same as for previous measurements with ^{107,109}Ag targets [8]. A 75-g sample of indium, enriched to 99.9% in ^{115}In, on loan from the ORNL Isotope Pool, was used. Neutron capture γ rays were detected by two coaxial intrinsic Ge crystals of 70% efficiency (relative to the ^{60}Co 1333-keV line). The amplitude information from the Ge detectors was measured with two 8k fast ADCs over the γ-ray energy range 0.1–7.2 MeV, in coincidence with the TOF information, measured with a 25-bit multiple-shot time digitizer. The data were recorded in an event-by-event mode on a 1-Gbyte hard disk of a PC-based data acquisition system. The neutron energy range from 3 to 480 eV was covered and a total of 30 Gbyte of listmode data were collected over a period of 800 h.

III. DATA ANALYSIS

A. Transmission data

Resonance parameters were determined by analysis of the data summed over both helicity states. Background and dead time corrections were applied as described by Crawford *et al.* [19]. The shape analysis was performed with the code FITXS [20], which was written specifically to analyze the TOF spectra measured by the TRIPLE Collaboration. The multilevel, multichannel formalism of Reich and Moore [21] was used for the neutron cross sections, which were convoluted with the TOF resolution function studied in detail by Crawford *et al.* [19]. The final fitting function is written as

$$\mathcal{F}_t(t) = \left\{ B_t(t) \otimes \left[\frac{\alpha}{E^{0.96}} e^{-n\sigma_D(t)} \right] \right\} + \sum_{i=0}^{3} \frac{a_i}{t^i}, \qquad (2)$$

where $\sigma_D(t)$ is the Doppler-broadened total cross section, $B_t(t)$ is the instrumental response function (which includes line broadening due to the initial width of the pulsed beam, neutron moderation, finite TOF channel width, and neutron mean time for capture in the detector), $\alpha/E^{0.96}$ is an energy dependent neutron flux as measured by Smith *et al.* [22], and the second term represents a polynomial fit to the background. (The symbol $\otimes$ indicates a convolution.) Since the initial TOF spectra were taken with unknown detector effi-

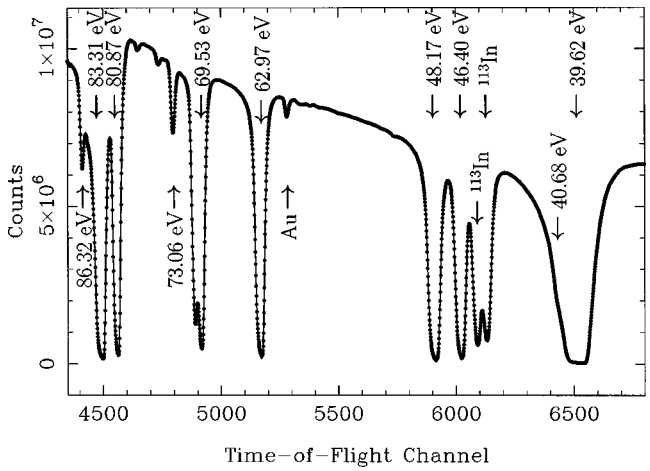

FIG. 1. Sample multilevel fit to the natural indium time-of-flight spectrum in the energy region 30–90 eV.

ciency and neutron flux, a normalization procedure was performed using well-known parameters of the 39.62-eV, 46.40-eV, and 62.97-eV indium resonances [23]. Details of the fitting procedures are given by Crawford *et al.* [19]. From this analysis the neutron resonance energies, $g\Gamma_n$ widths, and radiative widths can be obtained. A sample of a multilevel fit to the natural indium TOF spectrum in the energy region 30–90 eV is shown in Fig. 1.

After determining the resonance parameters and fixing them, the additional parameters $(f_n p)^+$ and $(f_n p)^-$ in the equations

$$\sigma^{\pm}_{pf_n} = \sigma_p[1+(f_n p)^{\pm}] \tag{3}$$

were fit separately for the + and − helicity TOF spectra. Here $\sigma^{\pm}_{pf_n}$ is the experimental neutron cross section for the + and − neutron helicity states (which is dependent on the beam polarization), and f_n is the absolute value of the neutron beam polarization. Because the f_n value is the same for the + and − cases, the quantities $(f_n p)^+$ and $(f_n p)^-$ should differ only by a sign, although statistical and systematic uncertainties may introduce further differences. The asymmetry p defined by Eq. (1) was calculated as

$$p = \frac{[(f_n p)^+ - (f_n p)^-]}{f_n[2+(f_n p)^+ + (f_n p)^-]}, \tag{4}$$

with the use of the f_n value obtained for each run from a proton magnetic resonance measurement. The NMR measurement is normalized to the result of a separate study of the well-known longitudinal asymmetry of the 0.74-eV resonance in lanthanum. The analysis to determine the PNC asymmetries in indium was performed on a run-by-run basis. A sample fit near the 29.6-eV resonance and the histogram of the p values obtained for this resonance are shown in Fig. 2.

B. Spin assignments

In order to determine the resonance spins, the low-level population method of spin assignment was used. This technique exploits the fact that the population of the low-lying excited states reached through γ-ray cascades from a neutron resonance depends strongly on the resonance spin and the spin of the excited state: the smaller the spin difference between the neutron resonance and a given final state of the cascade, the larger the population of the final state. The relative populations of the excited states are determined by measuring the intensities of the γ-ray transitions that deexcite them. In order to increase the sensitivity of the method and also to avoid normalization problems for the different resonances, it is convenient to measure the intensity ratio of two transitions depopulating levels of different spin. Usually a larger spin difference leads to a larger effect. In the past, as reviewed in [23], this method was successfully applied to a number of nuclei to determine the spins of *s*-wave resonances. This method has been successfully extended to *p*-wave resonances for the nuclides ^{238}U [24], ^{113}Cd [24], ^{107}Ag [8], and ^{109}Ag [8].

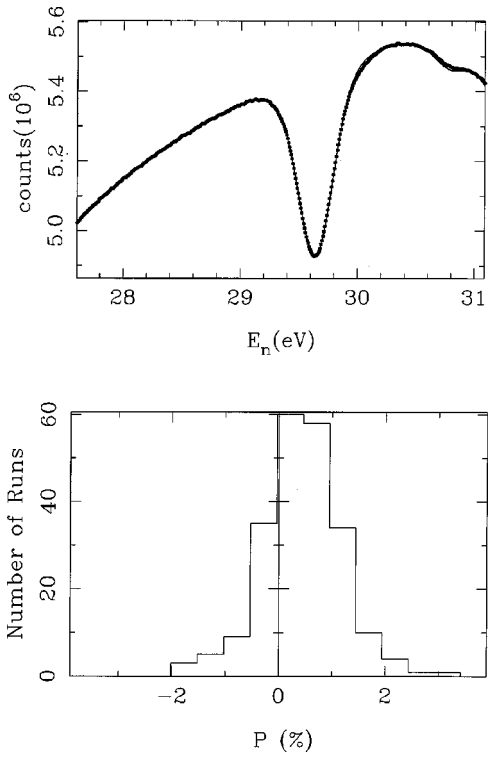

FIG. 2. Top: sample fit near the 29.68-eV resonance. Bottom: histogram of the asymmetries for the 29.68-eV resonance in ^{115}In.

From the recorded indium data, 140 capture γ-ray spectra (corresponding to the TOF intervals of indium resonances or background regions) were sorted. The TOF spectrum in the energy range 3–480 eV is shown in Fig. 3. The energies of the resonances analyzed are indicated, with the *p*-wave resonance energies underlined. In order to obtain the pure capture spectrum of a given resonance, the γ spectrum corresponding to one or more nearby background regions was subtracted from the raw data. For unresolved resonances, the yield was fit with the shape program FANAC [25]. For each resonance the contribution of the nearby resonance in the given TOF interval was determined and the corresponding γ-ray spectrum subtracted. This procedure was applied to

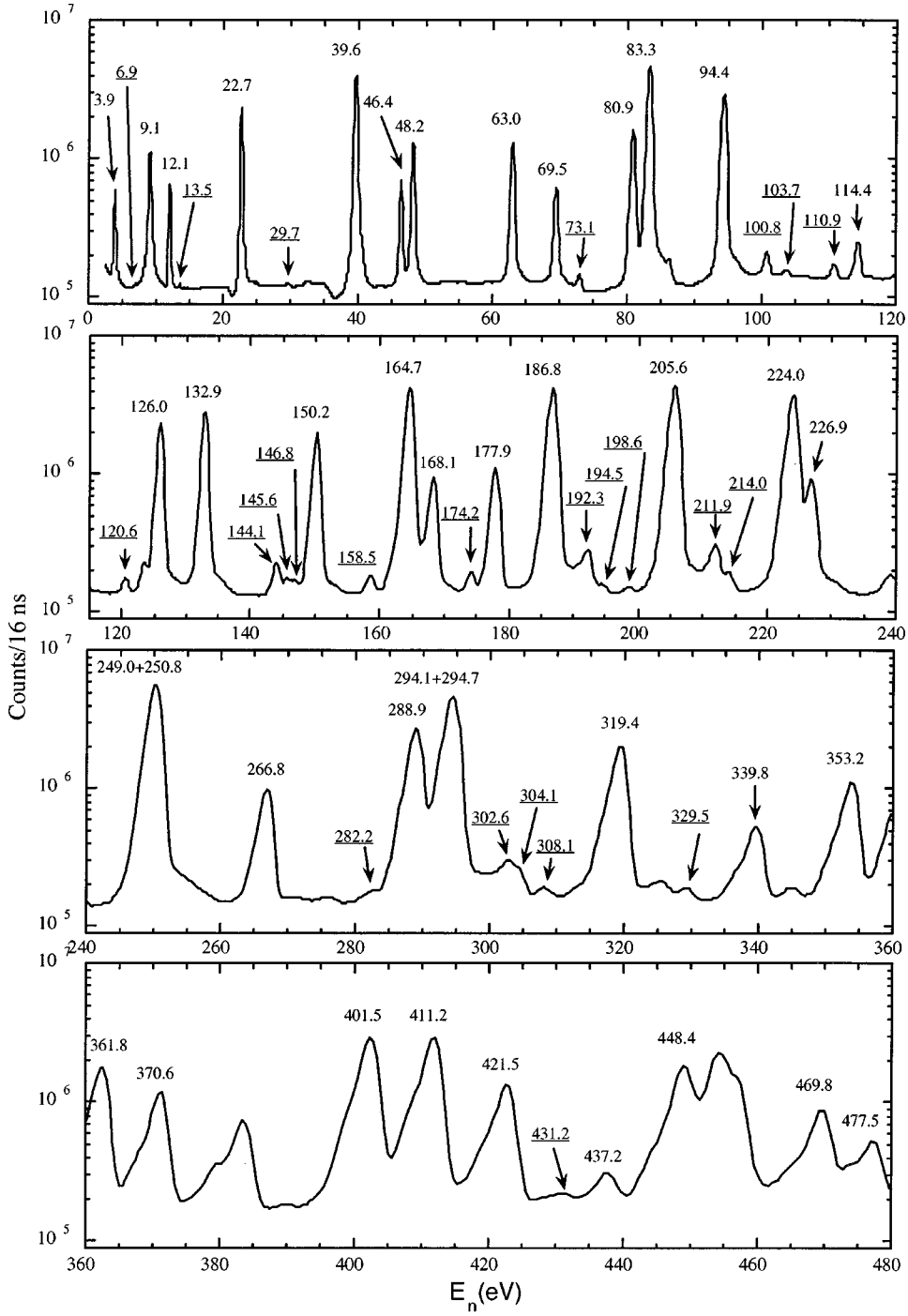

FIG. 3. Time-of-flight spectrum for ^{115}In(n,γ). The *p*-wave resonance energies are underlined. Resonance energies greater than 320 eV are from Ref. [29].

the *p*-wave resonances at 145.64, 146.78, 194.47, 282.2, 302.6, and 304.1 eV.

Low-energy γ-ray spectra for five resonances of different spin and parity are shown in Fig. 4. The top two spectra are for *s*-wave resonances, while the others are for *p*-wave resonances. The spin effect in the relative intensities is observed for several transitions; because of their large intensities it is convenient to use the 186.2-keV transition that depopulates the 313.5-keV level $(4^+,5^+)$ and the 273.0-keV transition that depopulates the 273.0-keV level (2^+) of ^{116}In. Figure 5 shows the ratios of the intensities of these transitions for the *s*- and *p*-wave resonances. As expected, the resonances separate into several groups. The lowest group with ratios around 0.1 contains only *p*-wave resonances and are accepted as spin $J=3$ resonances. The second group has values of the intensity ratio around 0.4. This group is identified as resonances with $J=4$; it contains *s*-wave as well as *p*-wave resonances. A third group shows a larger variation of the ratio around 0.8 and also contains *s*-wave and *p*-wave resonances. These are identified as resonances with spin $J=5$. No group of reso-

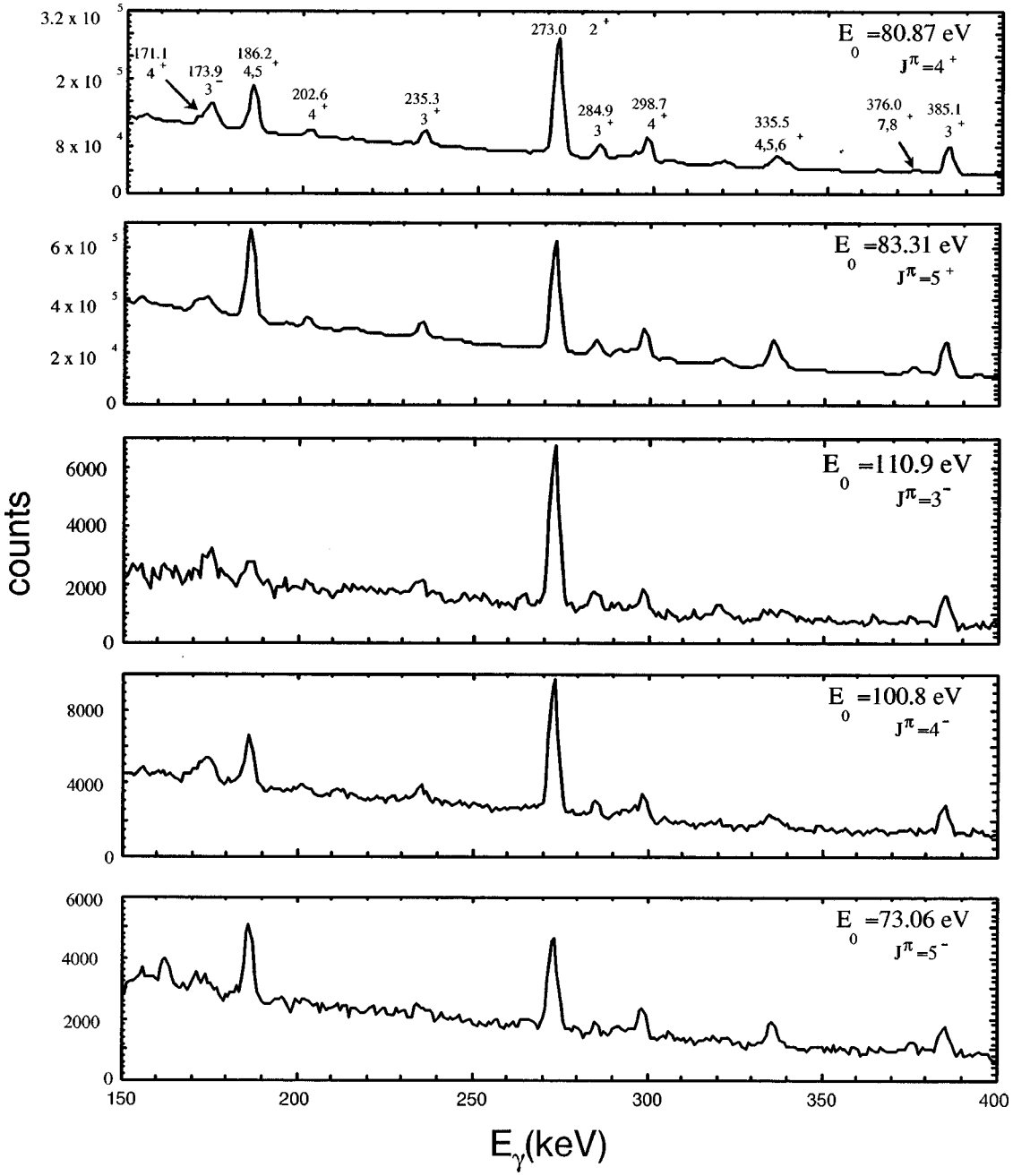

FIG. 4. Low-energy γ-ray spectra for five ^{115}In resonances of different spin and parity; the energies of the strongest transitions and the spins and parities of their initial levels are indicated.

nances with higher values of the ratio, as expected for spin $J=6$ *p*-wave resonances, has been observed.

Fluctuations of the intensity ratios are observed inside each group for both the *s*- and *p*-wave resonances, with the *p*-wave resonances displaying larger fluctuations. Besides contributions due to an imperfect background subtraction, to which the *p*-wave resonances are particularly sensitive, these fluctuations may be due to nonstatistical effects in the decay of the ^{116}In compound nucleus. The low-level population technique is based on the assumption that the γ decay from the capturing state is statistical. In the case of ^{115}In(n,γ) this assumption may not be completely justified since for some resonances rather strong primary transitions are observed to the low-lying levels used in the spin assignment. Two notable examples are the γ rays following capture at the 29.7-eV and 282.2-eV *p*-wave resonances. These resonances have a 5–10% primary transition of 6470.4 keV to the 313.5-keV level. Such direct feedings are subtracted before the ratio $I(186)/I(273)$ of the intensities of the 186.2- and 273.0-keV γ-ray transitions are determined.

Monte Carlo simulations of level populations based on the DICEBOX [26] code have been performed. Resonances with the same spin but different parities show equal values for the ratios in these simulations. In addition, the simulations predict an increase of the ratio $I(186)/I(273)$ with spin. The simulations also predict a larger value of this ratio for 6^-

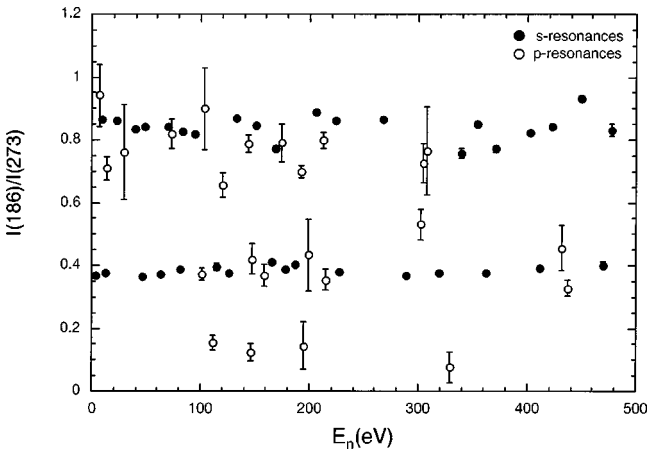

FIG. 5. Intensity ratios between the indicated γ-ray transitions plotted versus neutron energy for *s*-wave (solid circles) and *p*-wave (open circles) resonances in ^{115}In.

resonances. There are no 6^- *p*-wave resonances observed. One possible reason might be that such resonances can populate the 8^- isomeric state at 289.7 keV of ^{116}In easier than the lower-spin *p*-wave resonances. Therefore, a large fraction of the decays after neutron capture would be lost; that is, the selected low-energy transitions do not occur for 6^- resonances.

Other intensity ratios have been studied, notably $I(376)/I(385)$ and $I(186)/I(171+174)$. A comparison of $I(186)/I(273)$ with $I(376)/I(385)$ in Fig. 6 for *s*-wave resonances shows two groups of clustering values; one is related to $J=4$ and the other group to $J=5$ resonances. These intensity ratios cannot be used systematically for the *p*-wave resonances, because of the lower intensities of the γ-ray transitions. However, for the stronger *p*-wave resonances they can be used to support the J assignment based on the ratio $I(186)/I(273)$. For instance this is the case for the resonance at 302.6 eV, which has a higher value of $I(186)I(273)$ compared to the other $J=4$ resonances; the $J=4$ assignment is strengthened on the basis of the $I(376)/I(385)$ ratio.

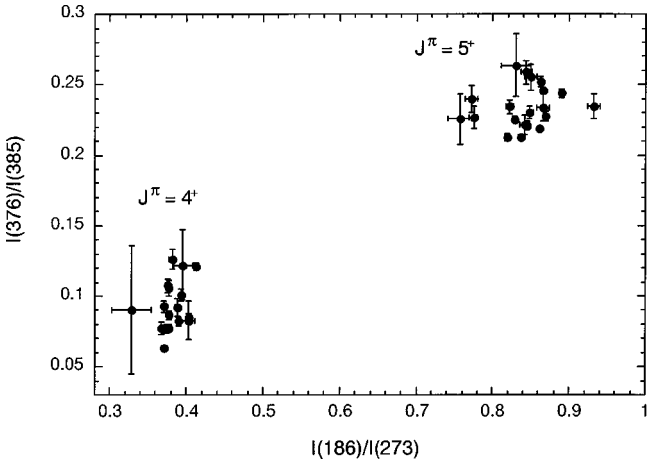

FIG. 6. Correlation between intensity ratios $I(376)/I(385)$ and $I(186)/I(273)$ for ^{115}In *s*-wave resonances.

High-energy primary transitions are also considered. In some cases the primary transitions help to assign spin and parity values to resonances. In addition, for the $J=5$ *p*-wave resonances, it is of interest to have information from primary transitions to ensure that no $J=6$ resonances are included in the same group. This is confirmed for the resonances at 6.85, 13.46, 73.06, 120.64, 144.07, 174.15, and 211.9 eV, for which direct transitions to levels with $J^\pi=4^+$ are observed. For the other resonances the statistics available is in general too low to allow the observation of high-energy transitions.

In Table I the values $I(186)/I(273)$ are given for the *p* resonances. Also the energies of the observed primary transitions, and the spin and parity of the final states, are indicated. Besides providing information on the resonance spins, they are useful for the resonance parity assignment, as discussed in the next section.

IV. EXPERIMENTAL RESULTS

A. Neutron spectroscopy data

Neutron resonance parameters, including spins, are listed in Table II. The energy scale was calibrated using the indium resonance energies from the compilation by Mughabghab *et al.* [23]. The orbital angular momentum l was assigned by two indirect methods: one uses a Bayesian probabilistic argument [27] and the other uses the decay properties of primary γ rays [12]. The first method applies Bayes' theorem to the Porter-Thomas distributions of neutron widths for *s*- and *p*-wave resonances. This method was extensively used in our *p*-wave neutron spectroscopic studies, e.g., by Smith *et al.* [22]. The second method is based on the observation of primary γ transitions to low-energy levels of known spin and parity. The ratio between the $E1$ and $M1$ photon strength functions for high-energy transitions for ^{116}In is about 6 [28]; therefore $E1$ transitions are more likely to be observed than $M1$. As shown in Table I, only high-energy transitions to levels with positive parity are observed for *p*-wave resonances, which is consistent with the $l=1$ assignment.

The neutron widths (the $g\Gamma_n$ parameters) show general agreement with those obtained by Frankle *et al.* [29]. There are a few cases (e.g., for the resonances at 58.76 eV, 86.3 eV, and 146.78 eV) where the widths differ by as much as a factor of 2. The origin of this discrepancy is unknown. However, these resonances are not important for our PNC study. The dominant uncertainties in the $g\Gamma_n$ and Γ_γ values shown in Table II are systematic, arising from the uncertainty in the count rate normalization and from the difference in our results for the two samples. Since the present results are in general agreement with the previous TRIPLE measurements [29], one expects the average resonance parameters to be little changed. The *s*-wave level spacing is $D_0=11.0\pm0.6$ eV. Assuming a ratio of $2J+1$ for the densities of *s*-wave spins $J=4$ and $J=5$, 45% of the *s*-wave resonances should have $J=4$ and 55% $J=5$. This leads to the result $D(J=4)=24.4\pm1.3$ eV and $D(J=5)=20.0\pm1.1$ eV, which we will use in Sec. V. Because of the new spin assignments, we obtained new information on the *s*-wave neutron strength function—namely, separate values for the J

TABLE I. Spin and parity assignment of ^{115}In p-wave resonances from high- and low-energy γ rays. The l_{HE} and J_{HE} are parity and spins on the basis of the observed high-energy transitions. The J_{LE} column gives spins based on the intensity ratio $I(186)/I(273)$ (second column).

E (eV)	$I(186)/I(273)$	γ primary observed (J^π of final level)	l_{HE}	J_{HE}	J_{LE}
6.853	0.94±0.10	5955.2 (4^+)	1	3,4,5	5
13.46	0.711±0.036	5814.0 ($3,4,5^+$), 6358.4 (4^+), 6656.3 (5^+)	1	4,5,6	5
29.68	0.76±0.15	6470.4 ($4,5^+$)	1		5
73.06	0.820±0.047	5752.8 (4^+)	1	3,4,5	5
100.81	0.373±0.019				4
103.70	0.91±0.13				5
110.86	0.157±0.023	6276.1 (3^+)	1	3,4	3
120.64	0.656±0.038	6559.3 (4^+)	1	3,4,5	5
144.07	0.788±0.027	5713.3 ($3,4,5^+$), 6358.4 (4^+), 6470.4 ($4,5^+$)	1	3,4,5	5
145.64	0.124±0.027	6039.5 (3^+)	1	3,4	3
146.78	0.421±0.049				4
158.53	0.368±0.034				4
174.15	0.792±0.060	6048.4 ($4,5^+$), 6559.3 (4^+)	1	3,4,5	5
192.29	0.698±0.020				5
194.47	0.146±0.075				3
198.6	0.43±0.11				4
211.9	0.800±0.025	5971.0 (4^+), 6470.4 ($4,5^+$)	1	3,4,5	5
214.0	0.356±0.035	6656.3 (5^+)	1	4,5,6	4
282.2	0.93±0.42	6470.4 ($4,5^+$)	1		4,5,6
302.6	0.531±0.048				4
304.1	0.726±0.062				5
308.1	0.76±0.14				5
329.5	0.078±0.048	5834.8 ($4,5^+$)	1		3
431.2	0.456±0.072				4
437.2	0.328±0.026				4

$=4$ and $J=5$ states: $S^0_{J=4}=(0.18\pm0.07)\times10^{-4}$ and $S^0_{J=5}=(0.22\pm0.07)\times10^{-4}$.

The PNC amplification parameters $A_{pJ}=\sqrt{\Sigma_s 4(g\Gamma^s_{nJ}/g\Gamma^p_{nJ})/(E_{sJ}-E_{pJ})^2}$ are listed for those p-wave resonances for which the longitudinal asymmetry was measured. They depend on knowledge of the spin J because the weak interaction mixes only p-wave and s-wave resonances with the same spin J. When the spins of the p-wave resonances are unknown, there are two entries for A_J, corresponding to the two possible spins $J=4$ and $J=5$ for which the ''weak mixing'' of levels is possible. The A_J values are zero for spins $J=3$ and $J=6$ because such p-wave resonances cannot exhibit parity violation.

B. Longitudinal asymmetries

As discussed in Sec. III, the histograms of the PNC asymmetry values for individual runs were plotted for each resonance. From these histograms a mean value of the asymmetry and its error were determined. The uncertainty in the mean value of p is the variance of the histogram divided by $N^{1/2}$. In this approach all errors contribute to the width of the histogram; as a result the histogram width gives a realistic estimate of uncertainty in the p value. The p values for the resonances which were analyzed are listed in Table II. There are nine statistically significant PNC effects. The longitudinal asymmetries are plotted versus energy in Fig. 7.

V. PNC ANALYSIS AND RESULTS

The details of the analysis of the PNC cross section asymmetries are given by Bowman *et al.* [30]. The specific application has been described in a number of our previous papers, e.g., our study of PNC effects in silver [8]. The essential argument is that the observed PNC effect in the p-wave resonance is due to contributions from neighboring s-wave resonances. Assuming that the weak matrix elements connecting the opposite parity states are random variables leads to the result that the longitudinal asymmetry is also a random variable. From the distribution of the asymmetries one can infer the variance M^2 of the matrix elements — this is the mean square matrix element of the PNC interaction. The practical details of the analysis depend on knowledge of the spectroscopic parameters. The essence of our approach to the likelihood analysis is to include all available spectroscopic information and to average over remaining unknowns. The net result is that more information reduces the uncertainty in the rms value of the matrix element. We provide an explicit example of this below.

TABLE II. Longitudinal asymmetries and related resonance parameters for ^{115}In.

E(eV)	l	J	gΓ_n (meV)	Γ_γ (meV)	p (%)	$A_{J=4}$ (eV^{-1})	$A_{J=5}$ (eV^{-1})
1.457 [a]	0	5	1.670				
3.850	0	4	0.170[a]				
6.853±0.009	1	5	0.00023±0.00002		−1.45±0.11		67.4
9.12±0.01	0	5	0.80±0.08				
12.10±0.01	0	4	0.049±0.005				
13.46±0.02	1	5	0.00092±0.00009		0.61±0.07		20.3
22.73±0.02	0	5	0.449±0.045				
29.68±0.02	1	5	0.00112±0.00011		0.44±0.04		12.4
39.62±0.02	0	5	2.02±0.10	84±8			
40.68±0.02	1		0.0037±0.0009		−0.55±0.04	2.7	44.6
46.40±0.03	0	4	0.128±0.011	91±20			
48.17±0.03	0	5	0.264±0.032	85±18			
58.76±0.03	1		0.00033±0.00002		−0.52±0.38	17.0	16.5
62.97±0.03	0	4	0.358±0.026	97±14			
66.40±0.12 [b]	1		0.000040±0.000002				
69.53±0.03	0	5	0.158±0.008	123±27			
73.06±0.03	1	5	0.012±0.001		0.046±0.023		4.3
77.81±0.04	1		0.0016±0.0001		−0.63±0.16	13.7	17.6
80.87±0.04	0	4	0.65±0.05	104±19			
83.31±0.04	0	5	3.33±0.19	75±7			
85.46±0.04	1		0.0031±0.0008		0.13±0.23	6.8	31.0
86.32±0.04	1		0.002±0.001		−0.025±0.024	2.3	8.9
88.44±0.04	1		0.00085±0.00016		−0.22±0.65	8.8	2.9
94.37±0.04	0	5	1.40±0.07	78±10			
100.81±0.04	1	4	0.031±0.002		0.007±0.019	1.1	
103.70±0.2 [b]	1	5	0.0004±0.0002				
110.86±0.05	1	3	0.021±0.002		0.04±0.03	0	0
114.41±0.05	0	4	0.067±0.004				
120.64±0.05	1	5	0.027±0.002		0.115±0.031		1.9
125.97±0.05	0	4	1.59±0.08	93±20			
132.94±0.05	0	5	1.91±0.27	130±40			
144.07±0.06	1	5	0.084±0.009		−0.045±0.019		1.8
145.64±0.06	1	3	0.028±0.003		0.022±0.037	0	0
146.78±0.06	1	4	0.023±0.005		0.084±0.044	2.2	
150.24±0.064	0	5	1.74±0.14	90±13			
156.42±0.07	1		0.0051±0.001		−0.10±0.17	9.9	7.3
158.53±0.07	1	4	0.046±0.004		0.54±0.03	4.4	
162.23±0.07	1		0.072±0.007		−0.014±0.025	8.5	1.7
164.65±0.07	0	4	7.50±0.47	93±13			
168.11±0.07	0	5	0.90±0.12	100±18			
174.15±0.08	1	5	0.084±0.009		−0.034±0.028		1.6
177.90±0.08	0	4	1.2±0.2	116±42			
186.79±0.08	0	4	9.85±0.50	98±14			
190.91±0.09	1		0.021±0.002		0.05±0.13	10.8	4.0
192.29±0.09	1	5	0.19±0.03		0.03±0.03		1.4
194.47±0.09	1	3	0.035±0.008		−0.03±0.06	0	0
198.6±0.1	1	4	0.031±0.004		0.04±0.07	3.5	
205.6±0.1	0	5	14.2±1.7	74±27			
211.9±0.1	1	5	0.24±0.03		−0.058±0.026		2.7
214.0±0.1	1	4	0.076±0.010		0.15±0.04	1.6	
219.9±0.1	1		0.0077±0.0004		1.00±0.62	6.4	19.0
224.0±0.1	0	5	10.1±2.0	89±19			
226.9±0.1	0	4	2.1±1.3		77±17		

TABLE II. (*Continued*).

E(eV)	l	J	gΓ_n (meV)	Γ_γ (meV)	p (%)	$A_{J=4}$ (eV^{-1})	$A_{J=5}$ (eV^{-1})
246.7±0.1	1		0.057±0.012		−0.11±0.13	8.6	3.0
249.0±0.1 [c]	0	4,5	0.40±0.02	83±8			
250.8±0.1 [c]	0	4,5	17.26±0.86	72±11			
264.5±0.5 [b]	1		0.04±0.02				
266.8±0.2	0	5	2.21±0.11	97±46			
275.6±0.2	1		0.007±0.003		1.07±0.60	8.6	9.5
276.6±0.2	1		0.048±0.011		−0.06±0.10	3.3	3.6
282.2±0.2	1		0.050±0.003		0.032±0.098	5.0	4.8
285.1±0.2	1		0.027±0.014		−0.23±0.35	10.5	8.2
288.9±0.2	0	4	8.05±0.88	131±21			
294.1±0.2 [c]	0	4,5	15.06±0.75				
294.7±0.2 [c]	0	4,5	4.21±0.21				
302.6±0.2	1	4	0.177±0.019		−0.46±0.06	2.6	
304.1±0.2	1	5	0.42±0.24		−0.061±0.045		2.2
308.1±0.2	1	5	0.073±0.006		0.06±0.13		3.7
313.4±0.6	1		0.11±0.09				
316.2±0.2	1		0.05±0.03		−0.11±0.25	7.2	3.1
319.4±0.2	0	4	5.8±1.4				

[a]From Mughabghab *et al.* [23].
[b]From Frankle *et al.* [29].
[c]Components of doublet.

Since the rms PNC matrix element M may depend on J, we label the matrix element as M_J. If the spins are known (such as for the resonances with $J=5$), one can fit the Bayesian posterior probability function $L(M_J)$ separately to the matrix elements M_J using the equation

$$L(M_J)=P^0(M_J)\prod_\mu P^I(p_\mu|M_J A_{\mu J},a,\sigma_\mu), \tag{5}$$

where $P^0(M_J)$ is the assumed *prior* probability density function for M_J, P^I is the appropriate probability density function [Eq. (16) in Ref. [30]] with experimental asymmetry p_μ, and σ_μ is the corresponding uncertainty. The normalization is discussed below. Even in this favorable case, with all spins known, there is still the problem that the entrance channel neutron $j=3/2$ and $j=1/2$ amplitudes of resonances are unknown. This factor is accounted for statistically by using the average value of the ratio of $S^1_{3/2}$ and $S^1_{1/2}$ strength functions, which is described by the parameter a ($a=0.58$ for indium [31]).

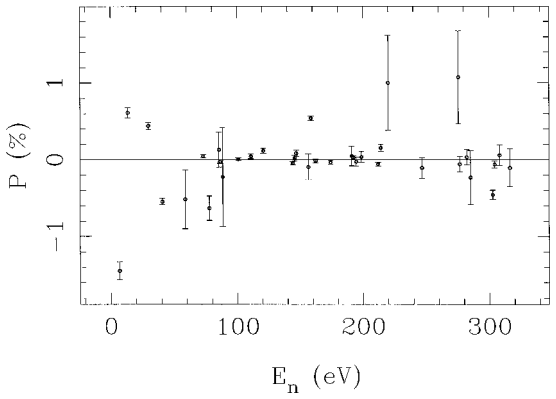

FIG. 7. Longitudinal asymmetries p versus neutron energies E_n for p-wave resonances in ^{115}In.

If there is incomplete information on the J values, one can fit to the weak spreading width

$$\Gamma_w=2\pi M_J^2/D(J), \tag{6}$$

assuming that Γ_w is independent of J. In this case the expression for the posterior probability function is

$$L(\Gamma_w)=P^0(\Gamma_w)\prod_\mu\left[\sum_{J=I\pm 1/2} p(J)P^I(p_\mu|M_J A_{\mu J},a,\sigma_\mu) + \sum_{J=I\pm 3/2} p(J)G(p_\mu,\sigma_\mu^2)\right], \tag{7}$$

where M_J is written as a function of Γ_w from Eq. (6), and $D(J)$ is a known parameter for spins $J=4$ and $J=5$. Additional quantities entering Eq. (7) are the relative probability $p(J)$ of spin J and a Gaussian G, which is the probability density function for resonances with spin $J=I\pm 3/2$ that cannot exhibit parity violation. The relative probabilities $p(J)$ are estimated using the standard statistical model for the J dependence; see, for example, the discussion by Bowman *et al.* [30]. Of course when J is known, then the probability vanishes for all except the one known J value.

The remaining issue is the normalization. In practice we assume that the prior $P^0(\Gamma_w)$ is a constant up to some value and zero above this value. Since we have measured weak spreading widths in a number of nuclei, we know that the

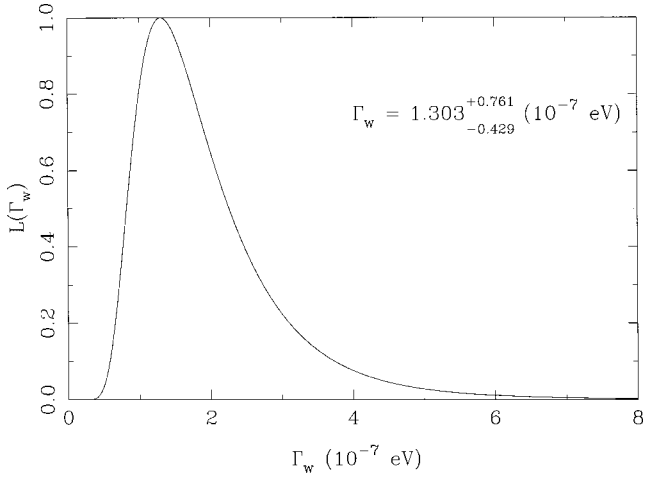

FIG. 8. Likelihood function L versus the weak spreading width Γ_w for p-wave resonances in ^{115}In with all available spin information.

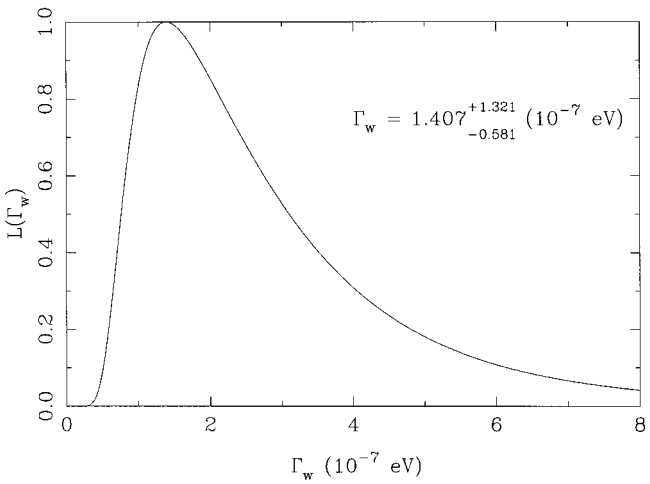

FIG. 9. Likelihood function L versus the weak spreading width Γ_w for p-wave resonances in ^{115}In without the spin information.

weak spreading width is unlikely to be more than about $(5-6)\times10^{-7}$ eV. For the present calculations we used the constant prior below 10×10^{-7} eV and zero above this value. We have determined empirically that the results are insensitive to the cutoff value chosen. Since the expression of Eq. (7) with a constant prior is a likelihood function, the uncertainties in Γ_w were obtained by the method of Eadie *et al.* [32] of the evaluation of the confidence interval by solving the equation

$$ln\left[\frac{L(\Gamma_w^{\pm})}{L(\Gamma_w^{*})}\right]=-\frac{1}{2}, \tag{8}$$

where Γ_w^* is the most likely value and $\Gamma_w^{\pm}$ gives the confidence range.

Our information on the spins of p-wave resonances in ^{115}In is not complete. Therefore, the likelihood analysis was performed using Eq. (7) with the data from both the J-known sets and the remaining J-unknown set. The resulting likelihood function is shown in Fig. 8. This case of maximum available spin information gives a value of $\Gamma_w=(1.30^{+0.76}_{-0.43})\times10^{-7}$ eV. As an example of the importance of the resonance spin assignments, Fig. 9 shows the likelihood functions for ^{115}In with all p-wave spin information omitted. Note that for this case the second term in each factor in Eq. (7) is always present and is independent of M (or Γ_w). This makes clear that it is the prior that ensures normalizibility. The width of the likelihood function for this case is a factor of 2 larger. Since there is little difference in the two values of $D(J)$ for $J=4$ and $J=5$, one can infer the M value from the weak spreading width using Eq. (6) with $D(J)=2D_0=22$ eV. This gives a value of $M=(0.67^{+0.16}_{-0.12})$ meV.

VI. SUMMARY

PNC longitudinal asymmetries have been studied for 36 p-wave resonances in ^{115}In. A total of nine p-wave resonances show parity violation with greater than 3σ statistical significance. Of these nine resonances five have positive signs and four have negative signs (relative to the sign of the PNC effect at 0.74 eV in lanthanum [1]). These results are consistent with a statistical distribution of the signs of the PNC effects. The value of the weak spreading width—$\Gamma_w=(1.30^{+0.76}_{-0.43})\times10^{-7}$ eV—is comparable to the values obtained in ^{238}U and ^{232}Th, and thus consistent with a constant weak spreading width. However, our other measurements indicate the presence of local fluctuations in the weak spreading widths. The large spread in values of Γ_w in this mass region makes it difficult to provide a definitive statement about a global mass dependence.

ACKNOWLEDGMENTS

This work was supported in part by the U.S. Department of Energy, Office of High Energy and Nuclear Physics, under Grant Nos. DE-FG02-97-ER41042 and DE-FG02-97-ER41033. The work was performed at the Los Alamos Neutron Science Center at the Los Alamos National Laboratory. This facility is funded by the U.S. Department of Energy, Office of Energy Research, under Contract No. W-7405-ENG-36.

[1] V.P. Alfimenkov, S.B. Borzakov, Vo.Van Thuan, Yu.D. Mareev, L.B. Pikelner, A.S. Khrykin, and E.I. Sharapov, Nucl. Phys. **A398**, 93 (1983).
[2] J.D. Bowman, G.T. Garvey, Mikkel B. Johnson, and G.E. Mitchell, Annu. Rev. Nucl. Part. Sci. **43**, 829 (1993).
[3] C.M. Frankle, S.J. Seestrom, N.R. Roberson, Yu.P. Popov, and E.I. Sharapov, Phys. Part. Nuclei **24**, 401 (1993).
[4] V.V. Flambaum and G.F. Gribakin, Prog. Part. Nucl. Phys. **35**, 423 (1995).
[5] G.E. Mitchell, J.D. Bowman, and H.A. Weidenmüller, Rev. Mod. Phys. **71**, 445 (1999).
[6] E.I. Sharapov *et al.*, Phys. Rev. C **59**, 1131 (1999).

[7] D.A. Smith *et al.*, Phys. Rev. C **60**, 045502 (1999).
[8] L.Y. Lowie *et al.*, Phys. Rev. C **59**, 1119 (1999).
[9] S.J. Seestrom *et al.*, Phys. Rev. C **58**, 2977 (1998).
[10] E.I. Sharapov *et al.*, Phys. Rev. C **59**, 1772 (1999).
[11] L.Y. Lowie, Ph.D. dissertation, North Carolina State University, 1996.
[12] L. Zanini, Ph.D. dissertation, Delft University, 1998.
[13] P.W. Lisowski, C.D. Bowman, G.J. Russell, and S.A. Wender, Nucl. Sci. Eng. **106**, 208 (1990).
[14] N.R. Roberson *et al.*, Nucl. Instrum. Methods Phys. Res. A **326**, 549 (1993).
[15] J.J. Szymanski *et al.*, Nucl. Instrum. Methods Phys. Res. A **340**, 564 (1994).
[16] S.I. Penttilä, J.D. Bowman, P.P.J. Delheij, C.M. Frankle, D.G. Haase, H. Postma, S.J. Seestrom, and Yi-Fen Yen, in *High Energy Spin Physics*, edited by K.J. Heller and S.L. Smith, AIP Conf. Proc. No. 343 (AIP, New York, 1995), p. 532.
[17] J.D. Bowman, S.I. Penttilä, and W.B. Tippens, Nucl. Instrum. Methods Phys. Res. A **369**, 195 (1996).
[18] Yi-Fen Yen *et al.*, Nucl. Instrum. Methods Phys. Res. A (to be published).
[19] B.E. Crawford *et al.*, Phys. Rev. C **58**, 1225 (1998).
[20] J.D. Bowman, Y. Matsuda, B.E. Crawford, and Y.-F. Yen (unpublished).
[21] C.W. Reich and M.S. Moore, Phys. Rev. **111**, 929 (1958).
[22] D.A. Smith *et al.*, Phys. Rev. C **59**, 2836 (1999).
[23] S.F. Mughabghab, M. Divadeenam, and N.E. Holden, *Neutron Cross Sections* (Academic, New York, 1981), Vol. 1, Pt. A.
[24] F. Gunsing, K. Athanassopulos, F. Corvi, H. Postma, Yu.P. Popov, and E.I. Sharapov, Phys. Rev. C **56**, 1266 (1997).
[25] F.H. Fröhner, Report No. KFK-2145, 1976. IRMM revised version by A. Brusegan (private communication).
[26] F. Bečvář, Nucl. Instrum. Methods Phys. Res. A **417**, 434 (1998).
[27] L.M. Bollinger and G.E. Thomas, Phys. Rev. **171**, 1293 (1968).
[28] F. Corvi and M. Stefanon, Nucl. Phys. **A233**, 185 (1974).
[29] C.M. Frankle *et al.*, Phys. Rev. C **48**, 1601 (1993).
[30] J.D. Bowman, L.Y. Lowie, G.E. Mitchell, E.I. Sharapov, and Yi-Fen Yen, Phys. Rev. C **53**, 285 (1996).
[31] L.V. Mitsyna, A.B. Popov, and G.S. Samosvat, in *Nuclear Data for Science and Technology*, edited by S. Igarasi (Saikon, Tokyo, 1988), p. 111.
[32] W.T. Eadie, P. Drijard, F.E. James, M. Roos, and B. Sadoulet, *Statistical Methods in Experimental Physics* (North-Holland, Amsterdam, 1971), p. 204.